L.C. Ingesson and D.J. Wilson

Optimization of Apertures and Collimators for Multi-Channel Plasma Diagnostics

Optimization of Apertures and Collimators for Multi-Channel Plasma Diagnostics

[1]A.L.C. Ingesson and [2]D.J. Wilson

[1]*FOM-Instituut voor Plasmafysica 'Rijnhuizen', Associatie Euratom-FOM, Trilateral Euregio Cluster, P.O. Box 1207, 3430 BE Nieuwegein, The Netherlands*
[2]*Euratom/UKAEA Fusion Association, Culham Science Centre, Abingdon, Oxon. OX14 3DB, UK*

Christian.Ingesson@jet.uk

ABSTRACT

Abstract Aperture, pin-hole and collimator detection systems are often used in plasma diagnostics, for example in soft x-ray detection and bolometer systems. In this paper the simultaneous optimization of viewing-beam overlap and light yield is considered in multi-channel aperture and collimator systems for two-dimensional (2D) tomography. This paper briefly highlights the relation between beam-width overlap and spatial aliasing in tomography, and how aliasing can be avoided in theory and in practice. Three-dimensional (3D) single-channel aperture and collimator systems can be approximated by a combination of two planar systems if the aperture is rectangular. Three ways to optimize beam-width overlap and light yield for planar aperture and collimator systems are considered in detail: overlap of the angular étendue at the Full-Width at Half-Maximum (FWHM), overlap of the geometric function at the FWHM a certain distance from the aperture, and arbitrary overlap for a given maximum beam width. The combination of 2D effects from all three optimization methods were used in the design of 3D apertures for a new mult i-channel bolometer camera on the JET (Joint European Torus) tokamak. The resulting apertures are complex, but the new camera has several advantages over the previous.

PACS numbers: 42.79.Ag, 52.70.-m, 42.30.Wb

I. INTRODUCTION

Apertures and collimators are used in radiation detection apparatus for parts of the spectrum for which no optical imaging components are available or are practical, such as in nuclear imaging, x-ray detection and bolometry. To avoid confusion in the following, "detection system" will always mean a single detector and one or more apertures, whereas "camera" will mean a collection of several detection systems. In this paper the optimization of apertures and collimators in cameras for tomography will be discussed, in particular for two-dimensional (2D) emission tomography in the field of plasma physics. Complex collimators have been designed in the medical tomography field, for instance for single photon emission computed tomography.[1,2,3] In plasma physics the apertures or collimators are usually relatively simple. In the past, apertures in cameras have been optimized for beam-width overlap for a given coverage,[4,5,6,7,8] but less attention has been given to optimizing the light yield. Here, the

simultaneous optimization of rectangular aperture or collimator systems in terms of several parameters will be discussed. Three-dimensional (3D) rectangular aperture and collimator systems can be described approximately as the combination of two independent planar (2D) systems. Although the underlying geometrical mathematics is simple, when apertures and collimators are optimized independently for two perpendicular planar systems the combined situation becomes quite complex. In non-rectangular aperture and collimator systems the geometrical description is far more complex [9] and it is more difficult to optimize various quantities simultaneously; this is outside the scope of this paper. The approximate separation of 3D aperture and collimator systems into two planar systems is particularly suited to 2D tomography of poloidal cross-sections on tokamaks and other fusion devices, but can also be applicable for tomography diagnostics in low-temperature plasma physics.

The structure of this paper is as follows. Section II introduces the quantities used in the optimization of aperture and collimator systems. Furthermore, it considers for which overlap of beam widths the level of spatial aliasing is acceptable in multi-channel cameras. Three different methods to optimize planar aperture and collimator systems are discussed in Sec. III. Section IV describes the consequences of these optimizations for the design of 3D systems for a bolometer camera on the JET (Joint European Torus) tokamak. The results are summarized in Sec. V.

II. CRITERIA FOR VIEWING-BEAM OVERLAP

In 2D tomography it is necessary to assume that the diagnosed quantity (here taken to be emission from an optically thin plasma) does not vary in the direction perpendicular to the reconstruction plane over a thickness that is measured by the 3D detection system (see Fig. 1 for the lay-out of detection systems and cameras). This thickness is determined by the aperture/collimator and detector sizes in this perpendicular direction. The maximum thickness for which this assumption is valid is an important parameter to optimize the light yield of the detection system. The aperture/collimator and detector sizes are also finite in the

reconstruction plane in order to achieve an acceptable light yield and signal-to-noise ratio; this leads to detectors viewing along beams of finite width. Other beneficial effects of finite beam widths in addition to a higher light yield are described below.

Convenient quantities to describe the beam widths in the reconstruction plane for 3D detection systems and how to use these in algorithms for 2D tomography have been described in Ref. 10: the angular étendue $e(\xi)$, the geometric function (in real space) $K(x,y)$ and the étendue E. These quantities can be expressed in terms of the geometric function *in projection space* $k(p,\xi)$.[9,10] Here p and ξ are parameters of a line of sight and are the distance from the line to a chosen origin and the angle between the line and the positive x axis, respectively. For a viewing direction in the reconstruction plane (p,ξ), the value of $k(p,\xi)$ reflects the properties of the viewing system in the direction perpendicular to the reconstruction plane. If the sizes of the detector and apertures of the detection system are small with respect to structures in the measured object, the angular étendue

$$e(\xi) = \int_{-\infty}^{\infty} k(p,\xi)\,\mathrm{d}p \qquad (1)$$

conveniently describes the beam shape as a function of viewing angle ξ. This is particularly useful if neighboring lines of sight form a viewing fan, i.e. if all average lines of sight of neighboring channels go through one point. The geometric function (in real space) describes the solid angle spanned by the entrance pupil of the detection system seen from the point (x,y), integrated over the direction perpendicular to the reconstruction plane, and can be calculated indirectly by[10]

$$K(x,y) = \int_0^\pi \int_{-\infty}^{\infty} k(p,\xi)\,\delta(p + x\sin\xi - y\cos\xi)\,\mathrm{d}p\,\mathrm{d}\xi, \qquad (2)$$

where δ is the Dirac delta function. Cross-sections of $K(x,y)$ in a direction perpendicular to the average viewing direction $\bar{\xi}$ give the functional shape of the beam width. The light yield of the detection system is characterized by its étendue, which is also called throughput, and can be obtained from the angular étendue by[10]

$$E = \int_0^\pi \frac{e(\xi)}{\cos(\xi - \bar{\xi})}\,\mathrm{d}\xi. \qquad (3)$$

If the detector and aperture in an aperture system are perpendicular and unshifted in the direction perpendicular to the reconstruction plane, the étendue can be approximated by[9]

$$E \approx \frac{16 D_p D_t P_p P_t}{L^2} \cos(\phi_d - \overline{\xi}) \cos(\phi_d - \overline{\xi}) = \frac{4 D_p P_p}{L} \cos(\phi_d - \overline{\xi}) \cos(\phi_d - \overline{\xi}) \frac{4 D_t P_t}{L} = E_p E_t , \quad (4)$$

where D and P are the half detector and aperture sizes, the subscripts p and t denote parallel and perpendicular to the reconstruction plane, the detector and aperture are at angles ϕ_d and ϕ_p, respectively, and L is the distance between the center of the detector and center of the aperture [see Fig. 2(a) for definitions of these symbols]. Expressions for some of these quantities for 3D rectangular aperture systems have been given elsewhere.[9] The approximate separation of the 3D aperture system into two planar systems is possible if the detector and aperture are rectangular and approximately parallel: in that case $k(p,\xi)$, i.e. the properties of the viewing system in the direction perpendicular to the reconstruction plane, is only a weak function of ξ.[9] When it is relevant, it will be indicated whether the quantities angular étendue and étendue are for a planar (2D) or 3D detection system. Equation (4) shows how the approximate 3D étendue can be separated into two 2D étendues.

For a planar aperture system [Fig. 2(a)] $k(p,\xi)$ will be 1 inside a region bounded by the curves defined in Fig. 2(b) and Table I, and 0 outside. Therefore, the 2D angular étendue is given by $e(\xi) = \Delta p(\xi)$, where $\Delta p(\xi)$ is the distance between the bounding curves in Fig. 2(b) at angle ξ (see the Appendix). Figure 2(c) shows the resulting 2D angular étendues. Expressions for the geometric function and étendue for a simple planar aperture system with the aperture parallel to the detector are given in the Appendix.

The quantities introduced above for individual detection channels are useful when considering an array of detectors in a camera. In the design of a camera the following interlinked criteria play a role: number of channels (cost), available space, required signal-to-noise ratio, required coverage and resolution. For a given number of channels and coverage (average lines of sight), the aperture or collimator systems can be optimized to give suitable beam widths and étendue. A larger beam width has the disadvantage of reduced resolution, but also has

advantages: 1) it is likely to give a larger étendue, 2) it reduces spatial aliasing in tomography, and 3) one avoids missing information about structures in the gaps between beam widths of adjacent channels. In particular in bolometry point 3 may be important if the total radiated power of a radiating object needs to be derived from the measurements. A beam-width overlap at full-width at half maximum (FWHM) as in Fig. 3(a) is suitable because the total radiated power can be obtained in principle by summing over adjacent channels. Traditionally, approximate overlap at FWHM has been achieved by overlaying the dashed lines of Fig. 2(a), which connect the center of the detector and the edges of the aperture, for neighboring detectors. In Sec. III it will be shown that in many cases this is a good approximation. Point 2 has been considered to some extent in the literature[11-13] and is discussed next for the application of bolometry on the JET tokamak.

The present vertical bolometer camera on JET[4] has an array of 14 detectors that view a poloidal cross-section of the plasma through one "pin-hole" aperture at location (x_{ap}, y_{ap}). The lay-out of this camera is similar to its replacement camera shown in Fig. 8 (normal view). One can define an aperture curve as $p_{ap}(\xi) = -(x_{ap} - x_0)\sin\xi + (y_{ap} - y_0)\cos\xi$, which describes all lines of sight through the center of the aperture [here (x_0, y_0) is a chosen origin]. The normalized 3D angular étendues of the channels of this camera are shown in Fig. 4(b). The angular étendues of all channels are similar; the reason for the variation in width and height is a cosine-effect due to the angle at which the various detectors view through the aperture. In the following the angular étendue of one of the channels is assumed to be representative for all channels i: i.e. $e_i(\xi) = e(\xi - \bar{\xi}_i)$, where $\bar{\xi}_i$ is the angle of the average viewing direction of channel i. The blurred measurement of channel i, $\hat{f}_i$, can be approximated by the convolution of the pure line-integral measurements $f(p, \xi)$ along the lines parametrized by p and ξ, i.e.

$$\hat{f}_i = \hat{f}(p_{ap}(\bar{\xi}_i), \bar{\xi}_i) = \int_0^\pi e(\xi' - \bar{\xi}_i) f(p_{ap}(\xi'), \xi') \, d\xi' \, ,$$

because the emitting structures are large compared with the detector and aperture size, or more precisely: large compared with max(Δp). Figure 4(a) shows the effect of blurring by the

6

angular étendue simulated for a realistic assumed emission profile.[14] The peaks in the emission profile occur in the divertor at the bottom of the vacuum vessel.

The Fourier transform of $\hat{f}$ along the aperture curve is given by

$$\hat{F}(\varXi) = \int \hat{f}(p_{\mathrm{ap}}(\xi),\xi)\,\exp(-2\pi i\xi\varXi)\,\mathrm{d}\xi\,.$$

Although the variable ξ is periodic, and hence the corresponding frequency variable would be discrete, here the periodicity of ξ is irrelevant because the function that is Fourier transformed goes to zero at both low and high ξ. Therefore, the frequency variable $\varXi$ considered here is continuous. In Fourier space (for the coordinate along the aperture curve) the effect of the blurring and of the limited sampling by the detectors is very clear [Fig. 4(c)]. The values for $\varXi < 0.1\,\mathrm{deg}^{-1}$ correspond to the peak of radiation between 80° and 90°, whereas peaks for $\varXi > 0.15\,\mathrm{deg}^{-1}$ correspond to the fine structure. In this example the peak at $\varXi \approx 0.2\,\mathrm{deg}^{-1}$ is not sufficiently damped by the angular étendue [Fig. 4(d)] which leads to noticeable aliasing. However, the amplitudes that are affected by the aliasing are relatively small, about a factor of 5 below the zero-frequency component.

The angular étendues of neighboring channels overlap close to their half-maximum values [Fig. 4(b)], as was discussed above. However, the Fourier transform of the angular étendue has its first zero only at the Nyquist frequency $1/\Delta\xi$, where $\Delta\xi$ is the spatial sampling rate [see Fig. 4(d)]. Therefore, with this kind of limited overlap between angular étendues, noticeable aliasing can occur as discussed above [Fig. 4(c)].[11–13] The lobes of the Fourier transform of the angular étendue are so small that hardly any aliasing would occur if the overlap of the angular étendues were twice the current, i.e. the first zero of the Fourier transform of the angular étendue would coincide with half the Nyquist frequency. However, this would lead to a significantly reduced spatial resolution. Furthermore, Fig. 4(c) is an extreme case as in other cases the aliasing effect has been found to be much smaller. Therefore, the current overlap between the angular étendue appears to be a reasonable compromise between maximizing resolution and minimizing aliasing. As pointed out before,

this FWHM overlap is the optimum for the total radiated power determination. However, in analysing data one should always remember that aliasing can occur. Restoration or deblurring of the measurements is only possible if the sampling distance is much smaller than the beam widths.[13]

III. OPTIMIZATION OF BEAM-WIDTH OVERLAP FOR PLANAR APERTURE AND COLLIMATOR SYSTEMS

A. Background

In this section different types of solutions $P(L)$ are found for given beam-width overlap in planar (2D) aperture and collimator systems. Note that two of these planar systems can be combined into a 3D system. In the following, the *projected* detector and aperture sizes are considered: $D^{\perp} = D\cos(\phi_{\mathrm{d}} - \overline{\xi})$ and $P^{\perp} = P\cos(\phi_{\mathrm{p}} - \overline{\xi})$. Figure 2(c) shows that the functional description of the angular étendue depends on whether $P^{\perp} < D^{\perp}$ or $P^{\perp} > D^{\perp}$. Several branches of solutions of P as a function of L for given beam-width overlap will be described. For a simple aperture system, the given overlap cannot be maintained for $L < L_{P=0}$, i.e. the distance for which $P = 0$. However, the given overlap can be achieved for smaller L if one considers a collimator system instead. We only consider the simplest collimator system with walls parallel to the average viewing direction which extend all the way from the detector plane to the aperture plane [Fig. 3(b)]. For such a collimator system the same equations as for the aperture system can be used, with the difference that the detector surface is subdivided in a number of sub-detectors with the size of the collimator C, i.e. $D'^{\perp} = P^{\perp} = C$ is substituted for $D^{\perp}$ and $P^{\perp}$ in the equations. As a limiting case (the highest étendue that can be obtained) the collimator walls are assumed to be infinitely thin. With integer division there can be $n = D^{\perp}/C$ collimators on the detector surface; this we call the "integer collimator." One can also make use of the leftover collimator of size $C' = D^{\perp} - nC$ [see Fig. 3(b)]. Because $C' < C$, the beam width of that collimator is always narrower than the other beam widths and does therefore not affect the beam-width overlap criterion.

However, it slightly raises the resulting étendue. This type of collimator system we call "fractional collimator".

In this section simplified planar apertures and collimators are considered with $\phi_d = \phi_p = \overline{\xi}$ [see Fig. 2(a)] because this leads to simpler equations for which many properties can be considered analytically and deeper insight can be gained. However, the methods described are general and in Sec. IV they are applied to an aperture/collimator system for which $\phi_d \neq \phi_p \neq \overline{\xi}$. For convenience all distance quantities in this section are normalized to the (half) detector size (effectively $D = 1$ is chosen). The (half) aperture size P and two-dimensional étendue as a function of detector-to-aperture distance L is considered for this fixed detector size and given beam-width overlap. Three different types of beam-width overlap with neighboring channels are considered: overlap at the FWHM of the angular étendue, overlap at the FWHM of the geometric function, and fixed width of the angular étendue or geometric function. The parameters, such as beam width, used in the example figures in this section have been chosen such as to highlight the different features of the various optimization methods, and may be far from realistic values (as used in Sec. IV).

B. Overlap at FWHM of angular étendue

As indicated above, the angular étendue is the most useful quantity to describe the beam width in the case of adjacent lines of sight in the shape of a fan. In this section we would like to optimize the étendue while the angular étendues of adjacent channels overlap at the half maximum. From the Appendix, Fig. 2(a–b) and Table I it is clear that $\Delta p(\xi)$, and therefore also $e(\xi)$, have a complicated functional dependence on $\cos\xi$ and $\sin\xi$. However, Fig. 2(c) shows that $e(\xi)$ can be approximated very well by three straight lines. Therefore, for given separation between adjacent channels $\Delta\xi$, the overlap criterion can be expressed approximately as follows [see Fig. 3(a)]

$$\tfrac{1}{2}\left|\xi_4 - \xi_1\right| + \tfrac{1}{2}\left|\xi_3 - \xi_2\right| = \Delta\xi.$$ (5)

For the simple aperture system with $\phi_d = \phi_p = \overline{\xi}$ and the detector straight behind the aperture $\xi_1 = -\xi_4$ and $\xi_3 = -\xi_2$, and Eq. (5) can be written as

$$\arctan\left(\frac{P+D}{L}\right) + \left|\arctan\left(\frac{P-D}{L}\right)\right| = \Delta\xi .$$

Figure 5(a) shows three different solution branches for P as a function of L for a given $\Delta\xi$: the aperture solution with $P > D$ for $L > L_{P=D} = 2D/\tan\Delta\xi$, the aperture solution with $P < D$ for $L_{P=D} < L < L_{P=0} = D/\tan(\Delta\xi/2)$, and the collimator solution for $L < L_{P=D}$. The collimator branch is a straight line $C(L) = L\tan(\Delta\xi)/2$. For $L \gg P$ the asymptotic limit of the $P > D$ aperture branch is $P(L) \approx L\tan(\Delta\xi/2)$ [see Fig. 5(a)]. For small $\Delta\xi$ one has $\tan(\Delta\xi/2) \approx \tan(\Delta\xi)/2$ and thus $L_{P=0} \approx L_{P=D}$ and the collimator and $P > D$ aperture branches lying very close to the straight line of the asymptotic limit. The asymptotic limit corresponds to the dashed lines from the center of the detector in Fig. 2(a) and is thus equivalent to the beam-width overlap criterion that has been used regularly in the past. From the present analysis it is clear that this is a very good approximation for small $\Delta\xi$.

The approximate 2D étendue according to Eq. (4) has been calculated for the various solutions $P(L)$ and is shown in Fig. 5(b). The two branches for the collimator are what was defined as integer collimator and fractional collimator in the previous subsection. The discontinuities in the integer collimator curve correspond to increases in n as one goes to smaller L. It is easy to show that the 2D étendue has a limit $2D\tan(\Delta\xi)$ for $L \rightarrow 0$; note that this corresponds to infinitely many collimators and thus requires infinitely thin collimator walls. For some L the two-dimensional étendue has been calculated analytically (see Appendix) [points in Fig. 5(b)], which shows that the approximate 2D étendue of Eq. (4) is a very good approximation in most cases. The angular étendues for some of these L are shown in Fig. 5(c). The functional shape of the angular étendue for large L has $\xi_3 \approx \xi_4 \approx \Delta\xi/2$, thus almost square, whereas for $P \approx D$ it is almost triangular. The difference in angular étendue values for the $P > D$ and $P < D$ branches is also evident (solid and dashed line); because the functional shapes of the angular étendue for the two branches is similar, the $P > D$ will probably always be preferable because it results in a higher étendue.

10

C. Overlap at FWHM of geometric function

The overlap of the angular étendue as in the previous subsection is an average overlap along the viewing beam. If the distance between neighboring detectors is larger than the maximum beam width, the beams may not overlap physically at all, only the angles overlap. In some cases it may be better to require the beams to overlap at a certain location. Without loss of generality we take the origin in the center of the aperture and rotate the coordinate system such that $\bar{\xi} = \frac{1}{2}\pi$; this means that y is the distance to the aperture and x is the direction perpendicular to the beam. The new beam-width overlap criterion can then be stated as follows: cross-sections of the geometric functions of adjacent channels should overlap at distance y. Note that at other distances the overlap may be very different. Also in this case the distance between neighboring detectors will be neglected, but it can be included by increasing the width ΔF below appropriately.

The expressions for the geometric function in the Appendix are relatively complicated functions, but often these can be approximated by straight lines and thus one can consider the width without needing to take into account the functional dependence of the geometric function. The width of the geometric function at a distance y can be expressed in $x_1 \ldots x_4$ of Fig. 2(a) and the Appendix. The widths Δa and Δb are indicated in Fig. 3(a) and for a simple aperture system these are

$$\Delta b = x_4 - x_1 = 2(D + P)\frac{y}{L} + 2P \tag{6}$$

and

$$\Delta a = |x_3 - x_2| = \left| 2(D - P)\frac{y}{L} - 2P \right|.$$

The overlap for channel spacing ΔF as indicated in Fig. 3(a) is obtained if

$$\tfrac{1}{2}\Delta b + \tfrac{1}{2}\Delta a = \Delta F . \tag{7}$$

Solving P as a function of L [see Fig. 6(a)], one finds that an aperture solution only exists for $L > L_{\text{lim}} = 2Dy / \Delta F$ (i.e. when $\Delta a = 0$) and is given by

$$P = \frac{\Delta F}{2(1 + y/L)}. \tag{8}$$

This solution again corresponds to the dashed lines in Fig. 2(a). The collimator solution of course exists for $L < L_{P=D} = 2Dy/(\Delta F - 2D)$ and its functional dependence is the same as in Eq. (8) because it is independent of D.

Figure 6(b) shows the aperture, and integer and fractional collimator branches of the 2D étendues that follow from substituting Eq. (8) in (4). The limit $L \to 0$ in this case is $2D\Delta F/y$. The approximate values of the étendue agree very well with the analytically calculated ones. Some examples of cross-sections of the geometric function for different L are shown in Fig. 6(c) (the equations for the geometric function are given in the Appendix). For large L the shape of the geometric-function cross-section becomes more square (and low amplitude), whereas the collimator solution at small L gives more-triangular cross-sections.

D. Fixed overlap of base of geometric function or angular étendue

The previous two subsections discuss very specific criteria for the overlap of the angular étendue and the geometric function. In this subsection we consider fixed maximum width, i.e. fixed maximum angular extent $\Delta\xi$, or fixed maximum width Δb at a distance y. This criterion can be used to specify the maximum extent of single channels, or to specify an overlap in multi-channel systems to reduce aliasing (e.g. $\Delta b << \Delta F$, where ΔF is the distance between the average lines of sight of neighboring channels).

For maximum width Δb Eq. (6) gives at location y and distance L

$$P = \frac{\Delta b - 2Dy/L}{2(1 + y/L)}, \tag{9}$$

which only has solutions for $L > L_{P=0} = 2Dy/\Delta b$. A collimator solution exists for $0 < L < L_{P=D} = 4Dy/(\Delta b - 2D)$ and is found by equating $D = P = C$ in Eq. (6):

$$C = \frac{\Delta b}{2(1 + 2y/L)}.$$

These curves are shown in Fig. 7(a).

The maximum angle with $\Delta\xi$ gives, with $\xi_4 - \xi_1 = \Delta\xi$,

$$P = L\tan(\Delta\xi/2) - D,$$

which has solutions for $L > L_{P=0} = D/\tan(\Delta\xi/2)$. The collimator solution for $0 < L < L_{P=D} = 2D/\tan(\Delta\xi/2)$ is

$$C = L\tan(\Delta\xi/2)/2.$$

These curves are also shown in Fig. 7(a). The maximum angle width $\Delta\xi$ equivalent to Δb is given by $\tan(\Delta\xi/2) = \Delta b/(2y)$, thus one sees that $L_{P=0}$ is the same for both maximum Δb and $\Delta\xi$ solutions, and $L_{P=D}$ and the solutions $P(L)$ and $C(L)$ differ only by the term 1 or D in the denominator. For small L the solutions $P(L)$ and $C(L)$ are therefore very similar, but for large L they deviate significantly. If P is optimized for a given maximum $\Delta\xi$, the resulting Δb is $2P$ larger than if optimized for the equivalent maximum Δb.

Figure 7(b) shows the approximate 2D étendue for these solutions; for the collimator branch again the integer and fractional solutions are shown. The maximum $\Delta\xi$ solution goes asymptotically to $E_{max} = 4D\tan(\Delta\xi/2)$ for large L, whereas for L→0 the étendue goes to $D\Delta b/y = 2D\tan(\Delta\xi/2)$. Note that the étendue for maximum Δb has a maximum at $L_{max} = \left(2D + \sqrt{4D^2 + 2D\Delta b}\right)y/\Delta b$.

IV. OPTIMIZATION OF 3D APERTURE SYSTEMS

Ideally one has two degrees of freedom in the optimization of aperture systems in cameras: the distance L and aperture size P. Whether the optimization methods for beam width overlap and étendue described in Sec. III can be used in the design of aperture and collimator systems depends on the situation. Often the coverage by a multi-channel camera is chosen to be fan shaped, which can be achieved by one common aperture for all channels, see Fig. 1(c) (this is often called "pin-hole" camera). If one uses individual detectors that have no restrictions on their distance from the common aperture, the optimization methods of Sec. III can be used.

13

However, in many cameras arrays of detectors are used with fixed detector-to-detector distance. For a given fan coverage, this fixes the distance L, and one can just use the equations of Sec. III to find the P appropriate for the required beam overlap, or one can optimize the étendue, but not both simultaneously. This problem can be circumvented by having an individual aperture or a collimator for each channel [Fig. 1(b)].

Although collimators give étendues similar to or even better than aperture systems [Figs. 5–7(b)], there can be considerable technical complications. In reality collimators will always have finite wall thickness, which reduces the étendue. It may be more difficult to manufacture rectangular collimators than rectangular apertures. Depending on the wavelength range there can be light reflections on the collimator walls; this is a problem even for small wavelengths due to the grazing incidence. Many collimator systems will therefore require anti-reflection features. For example, the bolometer cameras mounted in the JET tokamak divertor use screw-threaded cylindrical holes as collimators.[9] Circular collimators, however, radically change the shape of the beam widths[9] and make it impossible to optimize the parallel and perpendicular directions independently. If space is available, an aperture system may be a more practical solution than using a collimator.

The following is a discussion of the design of a aperture systems for a bolometer camera on the JET tokamak. This new bolometer camera was designed to replace the camera for which an analysis was made in Fig. 4. For various reasons a pin-hole camera could not be implemented; the main reasons are now briefly given. To improve the signal-to-noise ratio the detectors should be cooled (resistor noise is low, low-noise cabling can be used, and the probing voltage of the bolometers can be higher than if not cooled); vacuum requirements on the JET tokamak necessitate the cooling system to be contained in a secondary vacuum. It was decided that to reduce costs the camera should be compact so that only one water-cooling and secondary-vacuum system would be needed for all detectors. A compact camera has the further advantage that it can be made to fit through standard vacuum flanges (in this case a DN225 flange), which gives the flexibility to easily mount and unmount the camera without

14

welding. The range of possible positions of pin-holes and angles of the detectors in such a compact camera is very limited and a regular coverage of the entire plasma cross-section could not be achieved. Therefore, individual apertures for each detector were needed. In addition, if a common pin hole were used for several groups of detectors, the detector-to-aperture distance required to obtain a reasonable coverage would reduce the achievable étendue by a factor of two (see discussion on Fig. 9 below). Three different views of the plasma were combined in one camera [Fig. 8(a)]: 1) a normal view with 16 channels covering the plasma cross-section in a similar (but slightly improved) way as the camera it replaces [cf. Fig. 4(b)], 2) a back-up coarse view of eight channels, which will make possible an accurate estimate of the total radiated power even if channels of the normal-view break, and 3) a fine view of the divertor region at the bottom of the vessel with 8 channels. The aim of the fine view is to better resolve peaks in emissivity in the divertor than at present [Fig. 4(a)].

The chosen detectors are the standard compact metal-absorber bolometers designed by IPP-Garching,[15] which are used on many fusion devices. These bolometers are in arrays of four detectors at fixed distances. As discussed, in the case of fixed detector-to-detector distance, individual apertures give the flexibility to optimize the beam-width overlap and étendue independently. Figure 9 shows the approximate 3D étendue as a function of distance L for a representative channel of the normal view. The approximate 3D étendue was found to be accurate within 1% when compared with the numerically calculated 3D étendue for some L (see Fig. 9). The parameters for this channel are $D_p = 0.65\,\mathrm{mm}$, $D_t = 1.90\,\mathrm{mm}$, $\phi_d \approx \phi_p = 241°$, $\overline{\xi} = 246.25°$, $\Delta\xi_p = 4.6°$ and $\Delta b_t(@y = 3.5\,\mathrm{m}) = 0.5\,\mathrm{m}$; in the toroidal direction the detector and aperture are parallel. The angular-étendue overlap at FWHM constraint was applied in the poloidal direction (Sec. III.B) and the maximum width in the toroidal direction (Sec. III.D). The maximum Δb_t in the toroidal direction was chosen such that toroidal bending is negligible at the maximum distance of the views (otherwise analysis of measurements is complicated and blurring may occur in tomographic reconstructions). The étendue is seen to peak at $L = 333\,\mathrm{mm}$ [Fig. 9(a)]. This peak is mainly the result of the beam-width criterion in the toroidal direction. The collimator solutions [Fig. 9(b)], which are

complicated combinations of poloidal and toroidal collimators, have reasonably large étendues, but could not be implemented because of the technical difficulties discussed above. Around its peak in the aperture branch, the étendue is a shallow function of L. This means that, because neighboring channels are similar, the same L can be chosen for all channels of the same view with hardly any loss of performance. Actually, due to space restrictions, $L = 195\,\text{mm}$ was taken. For this L the toroidal and poloidal aperture sizes can be calculated for all channels from Eq. (9) and by solving Eq. (5) for P_{p}, respectively. The coarse-view channels would have required a larger L for optimum étendue. But with the L optimized for the normal-view channels the étendue is typically two times that of the normal-view channels, so that the signal-to-noise ratio will be good also with this L. For the current camera parameters $L_{P_{\text{p}}^{\perp}=D_{\text{p}}^{\perp}} < L_{P_{\text{t}}=D_{\text{t}}}$; for a different set of parameters this could be reversed and the resulting étendue curves as a function of L would look quite different from Fig. 9.

Figure 10 shows the design of the individual apertures. The detectors view from the top. The apertures with the sizes optimized as discussed are at the bottom. These apertures are precision machined. To avoid cross-talk between channels, walls between channels are necessary from the aperture to the detector; in other words: collimators are required. Note that this meaning of collimator is different from the multiple parallel-wall collimators discussed in Sec. III. Plain walls would reflect light, due to the grazing incidence even if they were blackened. Therefore, a set of plates with holes were carefully designed by 3D CAD to prevent light reaching a detector from any other than its own aperture (Fig. 10). The holes in the plates and at the top of the collimator block have been designed with a suitable tolerance as not to bound the view. The plates and insides of the collimator block are blackened to prevent stray light. The resulting "collimator block" is complicated but can be manufactured by means of wire erosion. As stated, the height of the collimator block is close to the optimum L for the normal-view. The width (256 mm) is limited by the port-flange size. To obtain the required fan-coverage, for some channels the bounding aperture had to be on the side of the collimator block. Although this reduces the poloidal part of the étendue, the toroidal part could be increased by choosing a larger P_{t}, which is possible because the maximum y in the

plasma is smaller for these non-vertically viewing channels [see Fig. 8(a)]. In fact, to ease the manufacture of the collimator block the toroidal-aperture size was chosen to be the same for all channels of the same view.

To obtain a high resolution with the fine view in the divertor region, the poloidal size of the apertures of the fine divertor view was optimized to give optimum overlap of the geometric function in the divertor [i.e. solving Eq. (7) for P to give the equivalent of Eq. (8) for arbitrary ϕ_d, ϕ_p and $\overline{\xi}$]. Figure 8(b) shows the resulting angular étendues for the three views. It can be seen that, although the optimization was carried out separately with planar systems in the poloidal and toroidal directions, deviations due to 3D effects are small. The reason for the high angular étendue for normal-view channels that have apertures on the side of the collimator block is the relatively large toroidal aperture, which is the same for all channels as indicated above, for short L. It should be pointed out that the angular étendues of the normal view are more square than those of the old camera in Fig. 4(b), and thus that the normal-view is more prone to aliasing in tomography. However, the non-ideal anti-aliasing overlap is fully compensated by the fine-view that covers the only region where fine structure in the emission can be expected.

In addition to the reasons to design separate apertures given above, a collimator block also has other advantages. It is attached to an outer screen, electrically insulated from the bolometers, that can conduct halo currents during disruptions and thus protect the sensitive bolometers. This also means that the shielding and earthing of the camera could be optimized. In the JET and other tokamaks the same type of bolometers suffers from interference with lower-hybrid waves, which are used to heat and drive current in the plasma. Although this interference has been reproduced in the laboratory, the physical mechanism has not been conclusively identified. Because the interference almost always created a negative signal, interference on the cabling has been ruled out. The many apertures in the collimator block and smallest size comparable to the wavelength of the LH waves make it possible to minimize interference, for instance by introducing a conducting mesh in some of the apertures.

17

V. CONCLUSIONS

The design of multi-channel aperture and collimator systems for plasma diagnostics is not usually optimized for more than one parameter: either beam-width overlap or étendue (light-yield). For some applications beam-width overlap at the FWHM is advantageous. The level of spatial aliasing in tomography with this beam-width overlap has been considered in theory and in practice: it was found that for the present application the level of spatial aliasing is acceptable for beam-width overlap at the FWHM.

Three ways to optimize beam-width overlap and light yield for planar aperture and collimator systems have been considered in detail: overlap of the angular étendue at FWHM, overlap of the geometric function at FWHM a certain distance from the aperture, and arbitrary overlap for a given maximum beam width. The required beam-width overlap can be achieved for a range of detector-to-aperture distances with an aperture size that is a function of the distance. The maximum light yield determines the optimum distance.

The combination of 2D effects from all three optimization methods in 3D rectangular aperture systems has been discussed for the design of a new bolometer camera designed for the JET tokamak. The resulting apertures are complex, but the new camera has several advantages over previous cameras: optimized beam-width overlap, signal-to-noise ratio and extent of the view in the toroidal direction.

ACKNOWLEDGMENTS

APPENDIX: SOME ANALYTICAL EXPRESSIONS FOR PLANAR APERTURE SYSTEMS

In Ref. 9 some analytical expressions are given for a 3D aperture system. These are also valid for planar systems, by taking $k(p, \xi) = 1$ inside the region given by Fig. 2(b) and Table I, and zero outside. Therefore, Eq. (1) gives $e(\xi) = \Delta p(\xi)$, where $\Delta p(\xi)$ is the distance between the curves in Fig. 2(b), which are given by $p_h(\xi) = -(x_h - x_0)\sin\xi + (y_h - y_0)\cos\xi$ with (x_h, y_h) from Table I and (x_0, y_0) an arbitrary origin which cancels in $\Delta p(\xi)$. In addition, the 2D geometric function (in real space) can be expressed analytically. The geometric function has a different functional behavior in the various regions A, C and D in Fig. 2(a). Outside these regions the geometric function is zero. The boundaries of these regions can easily be expressed in terms of the angles ξ_ε given in Table I: for a given y the x coordinate of boundary ε is given by $x_\varepsilon(y) = x' + (y - y')/\tan\xi_\varepsilon$, where $(x', y') = (x_I, y_I)$ for $\varepsilon = 1$ or 2, and $(x', y') = (x_{III}, y_{III})$ for $\varepsilon = 3$ or 4. A further region B needs to be introduced beyond the crossing point of lines with ξ_2 and ξ_3 if $P^\perp < D^\perp$. In the simple aperture system discussed in Sec. III.C this is the case for $y > PL/(D - P)$. The 2D geometric function in point (x, y) can be expressed as the angle spanned from that point by the entrance pupil of the detection system. With $\tan\theta_h(x, y) = (y - y_h)/(x - x_h)$, the geometric function in the various regions is given by

$$K_{2D}(x, y) = \begin{cases} |\theta_{II} - \theta_{IV}| & \text{for } (x, y) \text{ in region A,} \\ |\theta_I - \theta_{III}| & \text{for } (x, y) \text{ in region B,} \\ |\theta_{II} - \theta_{III}| & \text{for } (x, y) \text{ in region C,} \\ |\theta_I - \theta_{IV}| & \text{for } (x, y) \text{ in region D,} \\ 0 & \text{elsewhere.} \end{cases}$$

This equation shows that the geometric function curve in Fig. 6(c) does not consist of straight lines, but that they are complicated goniometric functions. In practice, however, straight lines give a very good approximation. Some equations given here and in Table I may fail at certain orientations of the aperture system as arctan returns a value in the range $-\frac{1}{2}\pi \ldots \frac{1}{2}\pi$, while a value in the range $0 \ldots 2\pi$ is required. Minor obvious modifications to the equations are needed in such a case to give the correct result. For more-complicated systems and 3D systems the geometric function can be calculated numerically with Eq. (2).

For a simple planar aperture system, with parallel detector and aperture at distance L, the exact 2D étendue can be calculated with Eq. (3) to give

$$E = 2(P+D)\arctan\left(\frac{P+D}{L}\right) - 2(P-D)\arctan\left(\frac{P-D}{L}\right) + L\ln\left(\frac{L^2+(P-D)^2}{L^2+(P+D)^2}\right).$$

For $L \gg P, D$ the Taylor expansion of this function gives $4DP/L$, which is equivalent to the planar parts of Eq. (4). This limit is easily satisfied, as is shown by the agreement between the approximate and analytical 2D étendues in Figs. 5(b) and 6(b). It can be verified, with considerable computational effort, that the integral over cross-section of the geometric function perpendicular to the average viewing direction gives the same result at any distance (this is the conservation of the étendue[10]).

REFERENCES

[1]. R.N. Beck and L.D. Redtung, IEEE Trans. Nucl. Sci. **32**, 875 (1985)

[2]. B.M.W. Tsui and G.T. Gullberg, Phys. Med. Biol. **35**, 81 (1990)

[3]. A.R. Formiconi, Phys. Med. Biol. **43**, 3359 (1998)

[4]. K.F. Mast and H. Krause, Rev. Sci. Instrum. **56**, 969 (1985)

[5]. D.F. da Cruz and A.J.H. Donné, Rev. Sci. Instrum. **65**, 2295 (1994)

[6]. A.W. Leonard, W.H. Meyer, B. Geer, D.M. Behne, and D.N. Hill, Rev. Sci.Instrum. **66**, 1201 (1995)

[7]. M.A. Ochando, E. Mirones, C. Rueda, and P. Rodríguez, Rev. Sci. Instrum. **70**, 384 (1999)

[8]. I. Furno, H. Weisen, J. Mlynar, R.A. Pitts, X. Llobet, Ph. Marmillod, and G.P. Pochon, Rev. Sci. Instrum. **70**, 4552 (1999)

[9]. L.C. Ingesson, C.F. Maggi, and R. Reichle, Rev. Sci. Instrum. **71**, 1370 (2000)

[10]. L.C. Ingesson, P.J. Böcker, R. Reichle, M. Romanelli, and P. Smeulders, J. Opt. Soc. Am. A**16**, 17 (1999)

[11]. A. Macovski, Proc. IEEE 71, 373 (1983)

[12]. A.G. Lindgren and P.A. Rattey, Adv. Electron. Electron Phys. 56, 359 (1981)

[13]. R.N. Bracewell, J. Comput. Assist. Tomogr. **1**, 6 (1977)

[14]. L.C. Ingesson, "Comparison of methods to determine the total radiated power in JET," Report JET-R(99)06, JET Joint Undertaking, Abingdon, UK (1999)

[15]. K.F. Mast, J.C. Vallet, C. Andelfinger, P. Betzler, H. Kraus, and G. Schramm, Rev. Sci.Instrum. **62**, 744 (1991)

Tables

TABLE I Bounding points and angles of the aperture system shown in Fig. 2(a).

Point h	x_h	y_h	ξ range	Angle ε	$\tan \xi_\varepsilon$
I	$x_p + P\sin\phi_p$	$y_p - P\cos\phi_p$	$\xi_1 \to \xi_2$	1	$(y_I - y_{IV})/(x_I - x_{IV})$
II	$x_d + D\sin\phi_d$	$y_d - D\cos\phi_d$	$\xi_2 \to \xi_4$	2	$(y_I - y_{II})/(x_I - x_{II})$
III	$x_p - P\sin\phi_p$	$y_p + P\cos\phi_p$	$\xi_4 \to \xi_3$	3	$(y_{III} - y_{IV})/(x_{III} - x_{IV})$
IV	$x_d - D\sin\phi_d$	$y_d + D\cos\phi_d$	$\xi_3 \to \xi_1$	4	$(y_{III} - y_{II})/(x_{III} - x_{II})$
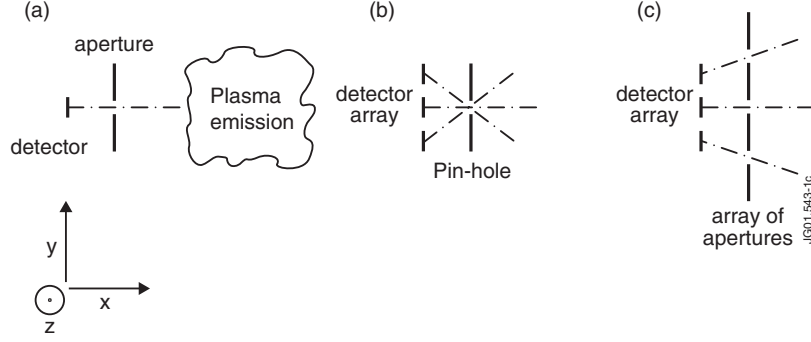
Fig.1: (a) Lay-out of a detection system in the xy reconstruction plane. The detector and aperture will also have a finite dimension in the perpendicular z direction; when the z direction is considered in addition to the xy plane the detection system will be referred to as three dimensional. (b) Schematic of a planar pinhole camera and (c) schematic of a planar camera with individual apertures for each detector. Note that in (c) walls are required between channels to avoid light from reaching a detector through other apertures.
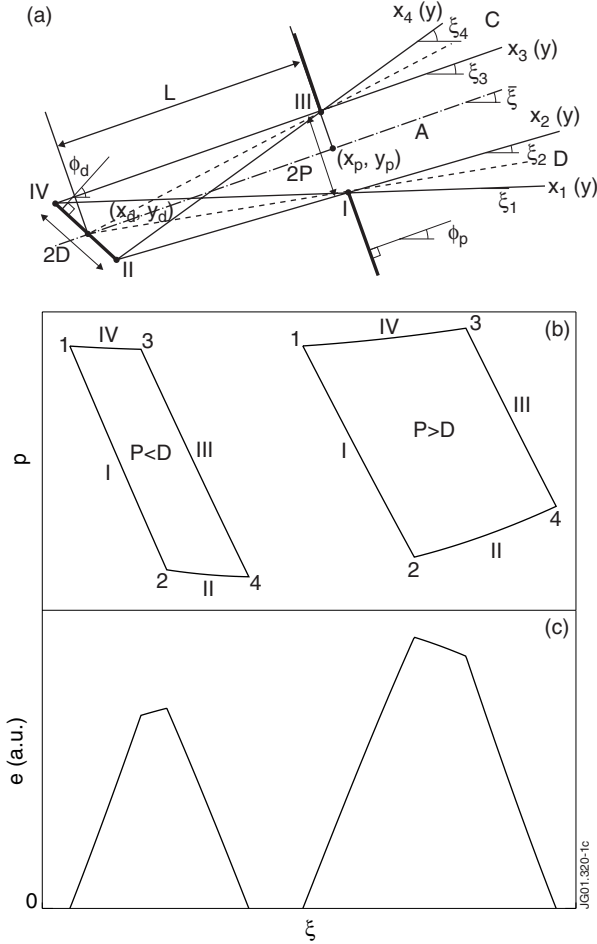
Fig.2: (a) Geometry of general planar aperture system and definition of quantities, points and regions. (b) Boundaries of nonzero region of $k(p,\xi)$ in projection space for two aperture systems with parallel detector and aperture of different relative sizes. The curves are defined in Table I. (c) The angular étendues corresponding to (b).
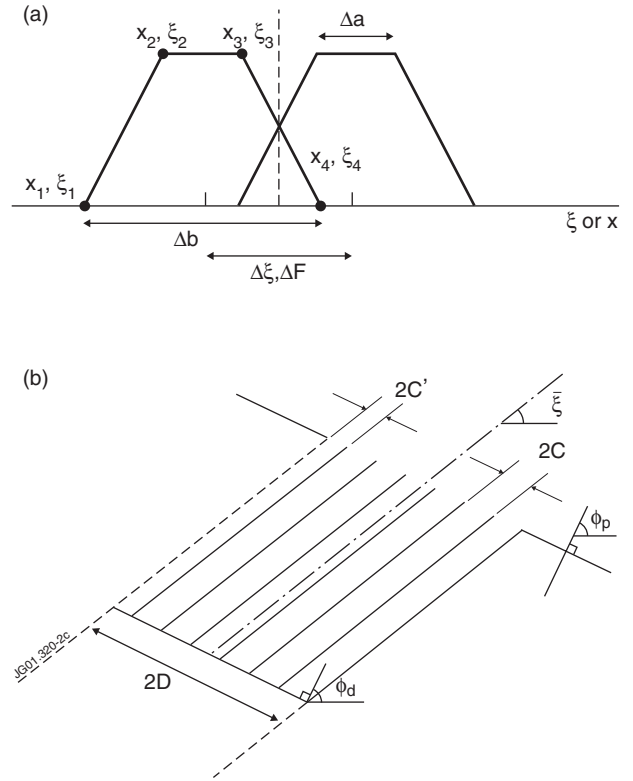
Fig.3: (a) Definition of quantities defining overlap of angular étendue and geometric function. (b) Illustration of parallel collimator system with infinitely thin walls. The collimator size is 2C and the leftover fractional collimator is indicated by 2C'.
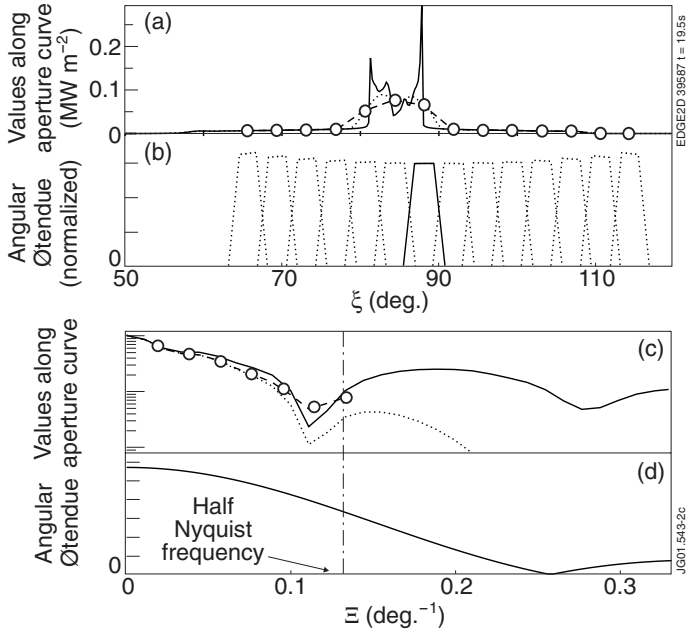
1

(a)

Values along aperture curve (MW m^{-2})

0.2

0.1

0

(b)

Angular Øtendue (normalized)

0

50   70   90   110

ξ (deg.)

EDGE2D 39567 t = 19.5s

Values along aperture curve

(c)

Angular Øtendue

(d)

Half
Nyquist
frequency

0

0   0.1   0.2   0.3

Ξ (deg.$^{-1}$)

JG01.543-2c

Fig.4: Quantities along aperture curve for a certain assumed emission profile as a function of the angle ξ (a,b) and its Fourier counterpart Ξ (c,d). (a) Solid line: line-integral values; dotted line: values blurred by angular étendue; circles: points where the blurred values are sampled (corresponding to the detectors); dashed curve: piecewise-linear fit to sampled points. (b) Angular étendue normalized to the étendue for the vertical KB1 detectors; the one used in the investigation is given by the solid line. (c,d) Fourier transforms of (a) and (b), respectively, with equivalent linetypes and symbols. Note that (c) is on a logarithmic scale and (d) on a linear scale. Although the Fourier transforms were carried out with the discrete Fourier transform (DFT), the number of samples was chosen such that the figures are a good representation of the analytical Fourier transform and that no inaccuracies were introduced due to the small number of samples and the fact that the samples do not extend over the entire range of the plasma. The dashed curve in (c) indicates the blurred function aliased with values higher than half the Nyquist frequency [$(2\,\Delta\,\xi\,)^{-1}$, where $\Delta\,\xi$ is the sampling rate; vertical dotdashed line at $\Xi =13\ deg^{-1}$]; the circles indicate the sampling points on the dashed curve.

(a)

2

1

0

P/D

P>D

P=D

P(L) = L tan($\Delta\xi$/2)

P<D

collimator

$L_{P=D}$ $L_{P=0}$ $\Delta\xi = 25^o$

1.0 (b)

fractional collimator

P>D

2D étendue (a.u.)

0.5

0

2Dtan $\Delta\xi$

integer collimator

P<D

0   5   10

L/D

2 (c)

angular étendue (a.u.)

1

0

$\Delta\xi$/2

0   10   20

ξ (deg.)

JG01.320-7c

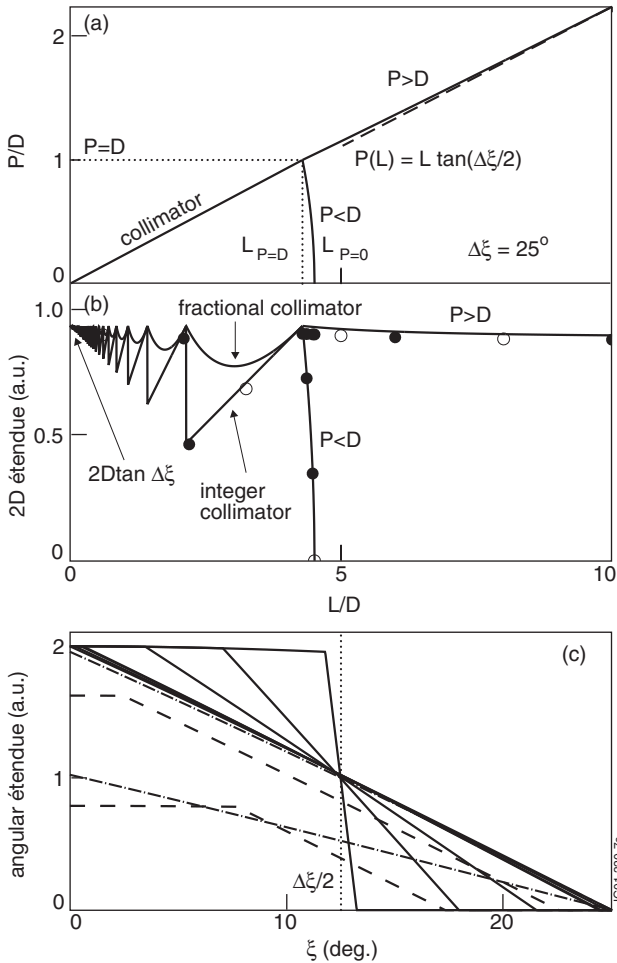*Fig.5: Results of optimized overlap of 2D angular étendue for angle difference $\Delta\xi = D\,25°$.(a) Optimum half aperture size P as a function of distance L. Three branches (apertures withD P > and D P < , and collimator) are indicated and the dashed line represents theasymptotic limit of the D P > solution for large L. Several critical points are identified in thefigure. (b) Approximate 2D étendue as a function of distance L for the three solution branchesfor P. The collimator branch has two curves: the integer collimator and fractional collimator. Analytically calculated étendues for some distances L are shown by open and solid circles. (c) Angular étendues for some distances L [solid circles in (b)] with the type of solution indicated by linestyle (solid: aperture D P > ; dashed: aperture D P < ; dot-dashed: collimator).*
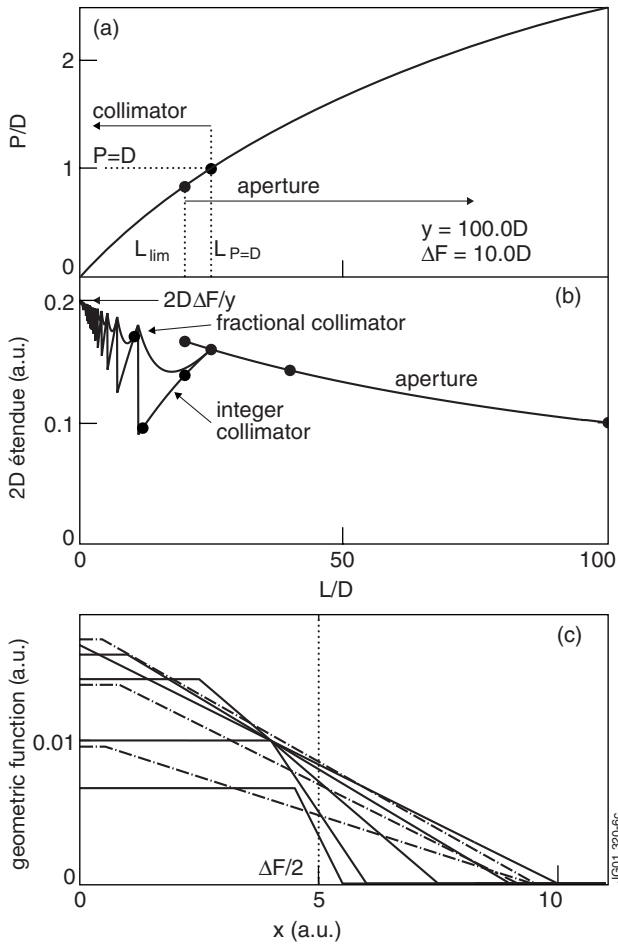
2

Fig.6: Results of optimized overlap of 2D geometric function $\Delta F 10 = D$ at a distance $D y 100 =$. (a) Optimum half aperture size P as a function of distance L. The aperture solutions and collimator solutions are indicated. Some critical points are identified in the figure. (b) Approximate 2D étendue as a function of distance L for the aperture and collimator solutions (integer and fractional collimators) of P. Analytically calculated étendues for some distances L are shown by solid circles. (c) Cross-section of geometric function at distance y as a function of x for some distances L with the type of solution indicated by linestyle (solid: aperture; dot-dashed: collimator).
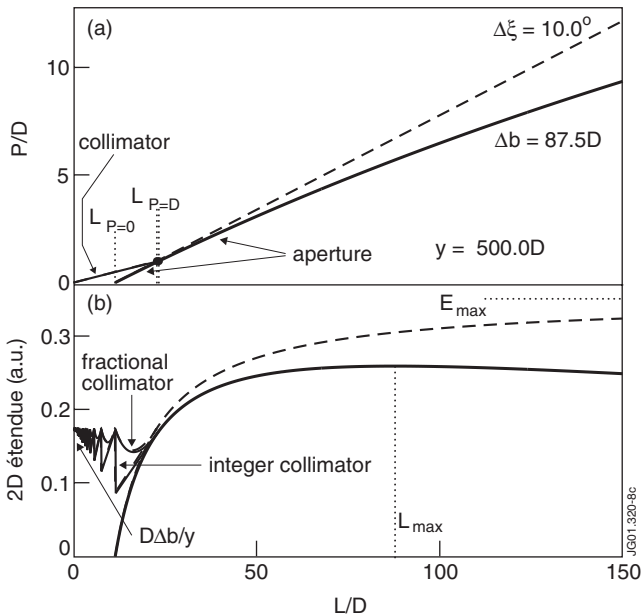
Fig.7: Results of optimized extent of geometric function (solid curves) and angular étendue (dashed curves) for $\Delta b= 87.5 D$ at a distance $y 500 =D$, which corresponds to an angle difference $\Delta \xi = D 10°$. (a) Optimum half aperture size P as a function of distance L. The aperture solutions and collimator solutions are indicated. Some critical points are identified in the figure. (b) Approximate 2D étendue as a function of distance L for the aperture and collimator solutions (integer and fractional collimator) of P.
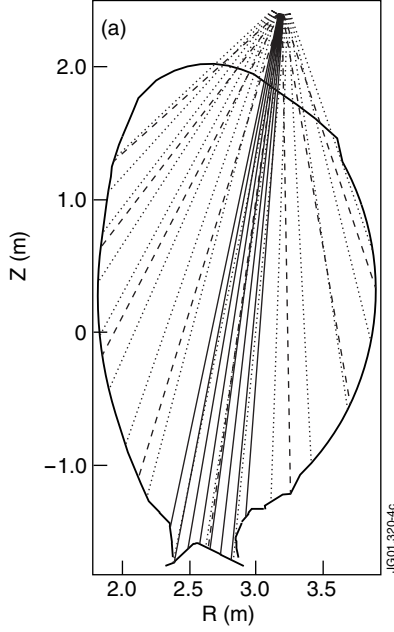
3

Fig.8: (a) Lines of sight and (b) 3D angular étendues of the new bolometer camera on the JET tokamak. Solid lines: fine view; dotted lines: normal view; dashed lines: coarse view. In (a) the wall surface closest to the plasma is indicated by a solid line. The bolometers are inside a vertical port.
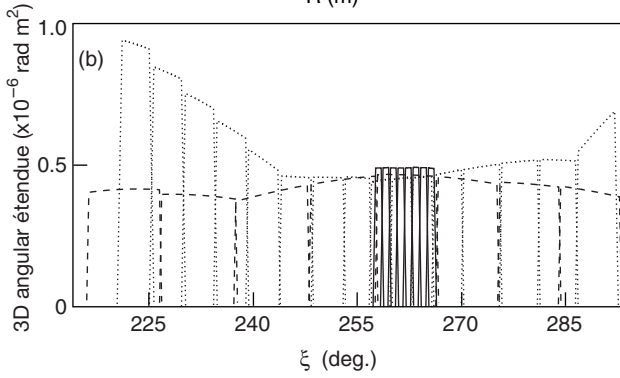

Fig.9: Results of optimized approximate angular étendue for a typical normal-view channel with poloidal angle difference $\Delta\xi_p = 6.4°$. The 3D étendue is shown as a function of distance L; (a) shows a large range and (b) shows a blow-up for small L. Above $L_{Pt=Dt}$ all solutions coincide. Below $L_{Pt=Dt}$ there are three toroidal solutions: the dashed line is the toroidal aperture solution, the solid line the toroidal integer collimator solution and the dot-dashed line the toroidal fractional collimator solution. For each of the toroidal collimator branches there is a poloidal aperture branch with $P_p^\perp > D_p^\perp$ for $L_{Pp\perp=Dp\perp}$, and a poloidal aperture branch with $P_p^\perp < D_p^\perp$ for $L_{Pp\perp=Dp\perp}<L<L_{Pp=0}$. Below $L_{Pp1=Dp1}$ there are two poloidal collimator branches; from top to bottom the four curves are: toroidal fractional collimator and poloidal fractional collimator, toroidal integer collimator and poloidal fractional collimator, toroidal fractional collimator and poloidal integer collimator, and toroidal integer collimator and poloidal integer collimator. For one of the branches (toroidal aperture or integer collimator and poloidal aperture or integer collimator) the numerically calculated 3D étendue for some L is plotted as solid circles.
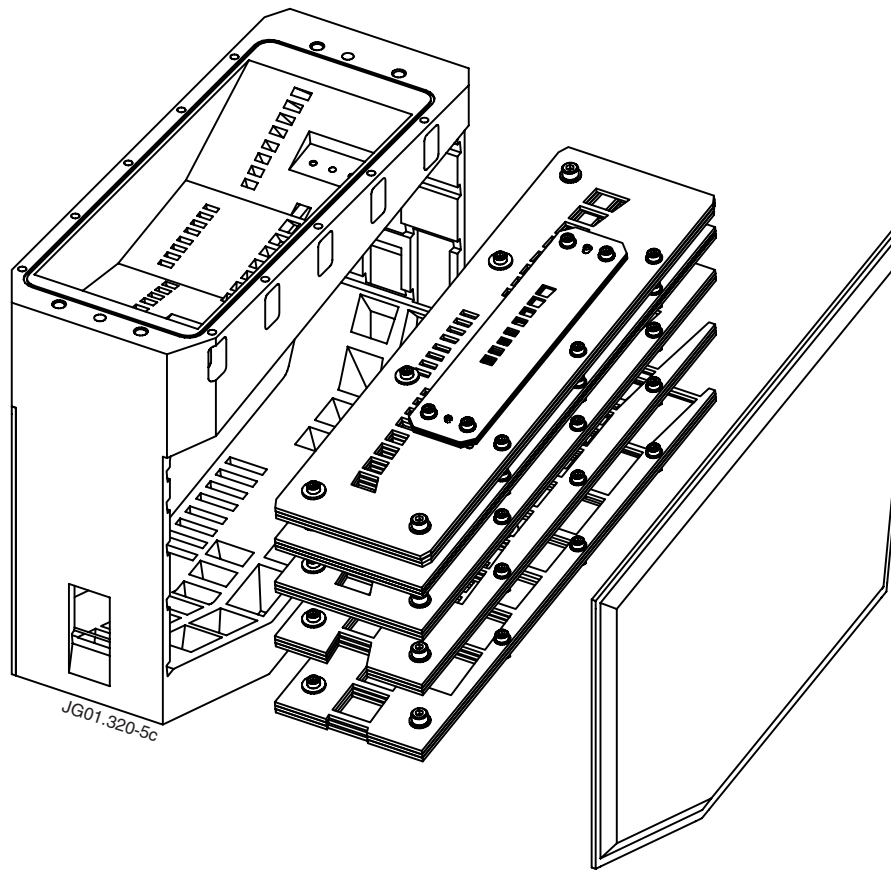
4
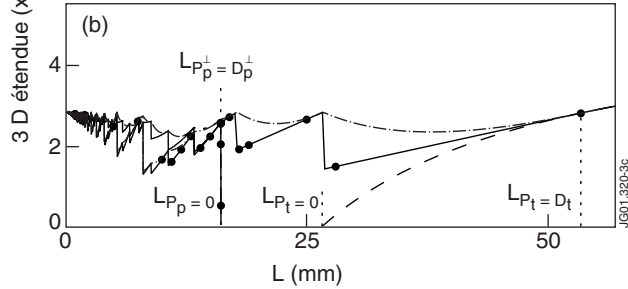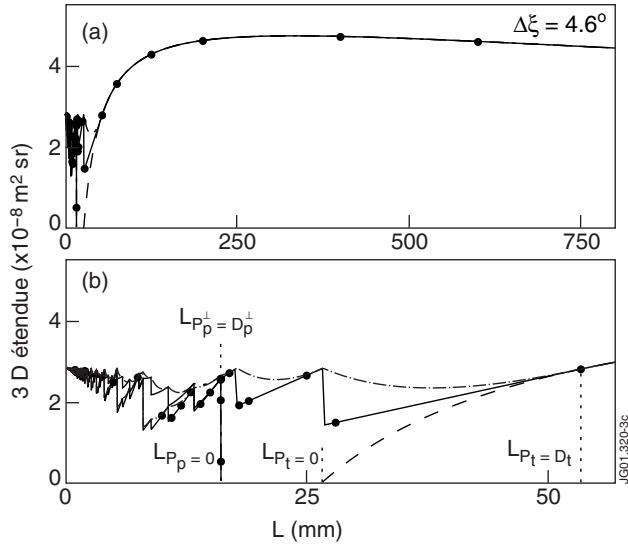
Fig.10: Expanded view of collimator block for a new bolometer camera on the JET tokamak. The detectors view from the top through a set of apertures. Fine view channels are at the left, normal-view channels in the middle and coarse-view channels at the right.